# Effects of Temporal Modeling on the Statistical Uncertainty of Spatiotemporal Distributions Estimated Directly from Dynamic SPECT Projections

Bryan W. Reutter, *Member, IEEE,* Grant T. Gullberg, *Senior Member, IEEE,* and Ronald H. Huesman, *Senior Member, IEEE*

*Abstract*— **Artifacts can result when reconstructing a dynamic image sequence from inconsistent single photon emission computed tomography (SPECT) projection data acquired by a slowly rotating gantry. The artifacts can lead to biases in kinetic parameters estimated from time-activity curves generated by overlaying volumes of interest on the images. To overcome these biases in conventional image based dynamic data analysis, we have been investigating the estimation of time-activity curves and kinetic model parameters directly from dynamic SPECT projection data by modeling the spatial and temporal distribution of the radiopharmaceutical throughout the projected field of view. In the present work, we perform Monte Carlo simulations to study the effects of the temporal modeling on the statistical variability of the reconstructed spatiotemporal distributions. The simulations utilize computationally efficient methods for fully four-dimensional (4-D) direct estimation of spatiotemporal distributions and their statistical uncertainties, using a spatial segmentation and temporal B-splines. The simulation results suggest that there is benefit in modeling higher orders of temporal spline continuity. In addition, the accuracy of the time modeling can be increased substantially without unduly increasing the statistical uncertainty, by using relatively fine initial time sampling to capture rapidly changing activity distributions.**

## I. Introduction

Artifacts can result when reconstructing a dynamic image sequence from inconsistent single photon emission computed tomography (SPECT) projection data acquired by a slowly rotating gantry. The artifacts can lead to biases in kinetic parameters estimated from time-activity curves generated by overlaying volumes of interest on the images. To overcome these biases in conventional image based dynamic data analysis, we and others have been investigating the estimation of time-activity curves and kinetic model parameters directly from dynamic SPECT projection data by modeling the spatial and temporal distribution of the radiopharmaceutical throughout the projected field of view [1–8].

In our previous work we developed a computationally efficient method for fully four-dimensional (4-D) direct estimation of spatiotemporal distributions from dynamic SPECT projection data [4], which extended Formiconi's least squares algorithm for reconstructing temporally static distributions [9]. In addition, we studied the biases that result from modeling various orders of temporal continuity and using various time samplings [4]. In the present work, we address computational issues associated with evaluating the statistical uncertainty of the spatiotemporal model parameter estimates, and use Monte Carlo simulations to validate a fast algorithm for computing the covariance matrix for the parameters and to study the effects of the temporal modeling on the statistical variability of the reconstructed distributions.

This work was supported by the National Heart, Lung, and Blood Institute of the US Department of Health and Human Services under grants R01-HL50663 and P01-HL25840, and by the Director, Office of Science, Office of Biological and Environmental Research, Medical Sciences Division of the US Department of Energy under contract DE-AC03-76SF00098. This work was developed in part using the resources at the US Department of Energy National Energy Research Scientific Computing (NERSC) Center.

B. W. Reutter and R. H. Huesman are with the Center for Functional Imaging, Lawrence Berkeley National Laboratory, University of California, Berkeley, CA 94720 USA.

G. T. Gullberg is with the Medical Imaging Research Laboratory, Department of Radiology, University of Utah, Salt Lake City, UT 84108 USA.

## II. Fast Computation of Statistical Uncertainty for Spatiotemporal Distributions

Following our development in [4], time-varying activity concentrations within volumes of interest encompassing the projected SPECT field of view can be modeled by selecting a set of temporal basis functions capable of representing typical time variations and having desired smoothness properties. Similarly, the spatially nonuniform activity concentration within a particular volume of interest can be modeled by selecting an appropriate set of spatial basis functions. Given a set of temporal basis functions and sets of spatial basis functions for the volumes of interest, coefficients for the resulting spatiotemporal basis functions can be estimated directly from the SPECT projection data, along with the covariance matrix for the coefficients.

### A. Covariance Matrix for the Spatiotemporal Basis Function Coefficients

Denoting the projection of the $m^{\text{th}}$ spatial basis function along ray $i$ at angle $j$ by $u_{ij}^m$, and the integral of the $n^{\text{th}}$ temporal basis function during the time interval associated with angle $j$ of rotation $k$ by $v_{jk}^n$, the projection equations can be expressed as

$$p_{ijk} = \sum_{m=1}^{M} \sum_{n=1}^{N} a_{mn} u_{ij}^m v_{jk}^n, \tag{1}$$

where the $p_{ijk}$ are the modeled projections, the $a_{mn}$ are the linear coefficients associated with the time integrals of the projections of the spatiotemporal basis functions, $M$ is the number of spatial basis functions, and $N$ is the number of temporal basis functions. The criterion which is minimized by varying the linear coefficients $a_{mn}$ is the weighted sum of squares function

$$\chi^2 = \sum_{i=1}^{I} \sum_{j=1}^{J} \sum_{k=1}^{K} \frac{(p_{ijk}^* - p_{ijk})^2}{W_{ijk}}, \tag{2}$$

where the $p^*_{ijk}$ are the measured projections, the $W_{ijk}$ are weighting factors, $I$ is the number of projection rays per angle, $J$ is the number of angles per rotation, and $K$ is the number of rotations. Typically, the weighting factors are either unity for an unweighted fit or the estimated variances of the projections for a weighted fit.

Equations (1) and (2) can be rewritten in matrix form as

$$\mathbf{p} = \mathbf{F}\mathbf{a} \tag{3}$$

and

$$\chi^2 = (\mathbf{p}^* - \mathbf{F}\mathbf{a})^{\mathrm{T}}\mathbf{W}(\mathbf{p}^* - \mathbf{F}\mathbf{a}), \tag{4}$$

respectively, where $\mathbf{p}$ is an $IJK$ element column vector whose $[i + (j-1)I + (k-1)IJ]^{\text{th}}$ element is $p_{ijk}$, $\mathbf{F}$ is an $IJK \times MN$ matrix whose $\{[i + (j-1)I + (k-1)IJ], [m + (n-1)M]\}^{\text{th}}$ element is $u^m_{ij} v^n_{jk}$, $\mathbf{a}$ is an $MN$ element column vector whose $[m+(n-1)M]^{\text{th}}$ element is $a_{mn}$, $\mathbf{p}^*$ is an $IJK$ element column vector whose $[i + (j-1)I + (k-1)IJ]^{\text{th}}$ element is $p^*_{ijk}$, and $\mathbf{W}$ is an $IJK \times IJK$ diagonal matrix whose $[i+(j-1)I + (k-1)IJ]^{\text{th}}$ diagonal element is $1/W_{ijk}$. The criterion, $\chi^2$, is minimized by the vector of spatiotemporal basis function coefficients

$$\hat{\mathbf{a}} = (\mathbf{F}^{\mathrm{T}}\mathbf{W}\mathbf{F})^{-1}\mathbf{F}^{\mathrm{T}}\mathbf{W}\mathbf{p}^*. \tag{5}$$

The covariance matrix for the coefficients $\hat{\mathbf{a}}$ is

$$\mathrm{cov}(\hat{\mathbf{a}}) = (\mathbf{F}^{\mathrm{T}}\mathbf{W}\mathbf{F})^{-1}\mathbf{F}^{\mathrm{T}}\mathbf{W}\mathrm{cov}(\mathbf{p}^*)\mathbf{W}\mathbf{F}(\mathbf{F}^{\mathrm{T}}\mathbf{W}\mathbf{F})^{-1}, \tag{6}$$

where $\mathrm{cov}(\mathbf{p}^*)$ is the covariance matrix for the measured projections. Given an estimate of $\mathrm{cov}(\mathbf{p}^*)$, estimates of the statistical uncertainties of the coefficients $\hat{\mathbf{a}}$ are the square roots of the diagonal elements of the covariance matrix given by equation (6) and are denoted individually by $\hat{\sigma}_{\hat{a}_{mn}}$. In general, the errors in the coefficients are correlated and the covariance matrix given by equation (6) has nonzero elements off the diagonal.

For an unweighted least squares reconstruction of the spatiotemporal basis function coefficients $\hat{\mathbf{a}}$ (i.e., for $\mathbf{W}$ an identity matrix), an estimate of the symmetric $MN \times MN$ covariance matrix $\mathrm{cov}(\hat{\mathbf{a}})$ can be obtained quickly from equation (6) as follows. Assuming Poisson noise, the diagonal matrix having the modeled projections $\hat{\mathbf{p}} = \mathbf{F}\hat{\mathbf{a}}$ along the diagonal can be used as an estimate of the covariance matrix for the measured projections. Substituting this diagonal matrix for $\mathrm{cov}(\mathbf{p}^*)$ and the identity matrix for $\mathbf{W}$, equation (6) can be rewritten as

$$\mathrm{cov}(\hat{\mathbf{a}}) = (\mathbf{F}^{\mathrm{T}}\mathbf{F})^{-1}\mathbf{F}^{\mathrm{T}}\mathrm{diag}(\mathbf{F}\hat{\mathbf{a}})\mathbf{F}(\mathbf{F}^{\mathrm{T}}\mathbf{F})^{-1}. \tag{7}$$

We have presented a method for quickly calculating $(\mathbf{F}^{\mathrm{T}}\mathbf{F})^{-1}$ in [4]. Using a similar development, the symmetric $MN \times MN$ matrix $\mathbf{F}^{\mathrm{T}}\mathrm{diag}(\mathbf{F}\hat{\mathbf{a}})\mathbf{F}$ can be calculated quickly as follows. Denoting the $\{[m + (n-1)M], [m' + (n'-1)M]\}^{\text{th}}$ element of $\mathbf{F}^{\mathrm{T}}\mathrm{diag}(\mathbf{F}\hat{\mathbf{a}})\mathbf{F}$ by $\psi^{mnm'n'}$, one has

$$\begin{aligned}\psi^{mnm'n'} &= \sum_{i=1}^{I}\sum_{j=1}^{J}\sum_{k=1}^{K} u^m_{ij} v^n_{jk} \times \\ &\quad \left[\sum_{m''=1}^{M}\sum_{n''=1}^{N} \hat{a}_{m''n''} u^{m''}_{ij} v^{n''}_{jk}\right] \times u^{m'}_{ij} v^{n'}_{jk},\end{aligned} \tag{8}$$

where $\hat{a}_{m''n''}$ is the $[m'' + (n''-1)M]^{\text{th}}$ element of $\hat{\mathbf{a}}$, and "$\times$" denotes scalar multiplication. Rearranging the summations yields

$$\begin{aligned}\psi^{mnm'n'} &= \sum_{m''=1}^{M}\sum_{n''=1}^{N} \hat{a}_{m''n''} \times \\ &\quad \sum_{j=1}^{J}\left[\sum_{i=1}^{I} u^m_{ij} u^{m'}_{ij} u^{m''}_{ij}\right]\left[\sum_{k=1}^{K} v^n_{jk} v^{n'}_{jk} v^{n''}_{jk}\right] \\ &= \sum_{m''=1}^{M}\sum_{n''=1}^{N} \hat{a}_{m''n''} \sum_{j=1}^{J} \alpha_j^{mm'm''} \beta_j^{nn'n''} \\ &= \sum_{m''=1}^{M}\sum_{n''=1}^{N} \hat{a}_{m''n''} \gamma^{mnm'n'm''n''},\end{aligned} \tag{9}$$

where the factors $\alpha_j^{mm'm''}$ and $\beta_j^{nn'n''}$ denote the summations $\sum_{i=1}^{I} u^m_{ij} u^{m'}_{ij} u^{m''}_{ij}$ and $\sum_{k=1}^{K} v^n_{jk} v^{n'}_{jk} v^{n''}_{jk}$, respectively, and the factor $\gamma^{mnm'n'm''n''}$ denotes the sum $\sum_{j=1}^{J} \alpha_j^{mm'm''} \beta_j^{nn'n''}$.

Using the factorization given by equation (9), it can be shown that most of the overhead associated with computing the symmetric matrix elements $\psi^{mnm'n'}$ lies in calculating the $\alpha_j^{mm'm''}$ factors and the $\gamma^{mnm'n'm''n''}$ factors. These calculations take about $[(I/N^3) + 1]JMNQ$ multiply-and-add operations, where $Q = (MN)(MN + 1)/2$. By comparison, relatively straightforward computation of the summations given by equation (8) takes about $IJKQ$ multiply-and-add operations. Thus, for the simulated dynamic cardiac cone beam SPECT studies described in Section III, for which $I/N^3$ = 1/2, the factorization given by equation (9) reduces the computation by a factor of about $2IK/3MN \approx 200$.

### *B. Covariance Between Integrated Time-Activity Curve Model Segments*

Given an estimate of $\mathrm{cov}(\hat{\mathbf{a}})$, the covariance matrix for the spatiotemporal basis function coefficients, estimates of the covariance between integrated segments of the time-activity curve models for the volumes of interest can be obtained as follows.

The integral of the time-activity curve model for volume of interest $m$, during the time interval associated with angle $j$ of rotation $k$, can be expressed as $\sum_{n=1}^{N} \hat{a}_{mn} v^n_{jk}$. Thus, the covariance of this time integral with the time integral associated with volume of interest $m'$ during angle $j'$ of rotation $k'$ is

$$\begin{aligned}&\mathrm{cov}\left(\sum_{n=1}^{N} \hat{a}_{mn} v^n_{jk}, \sum_{n=1}^{N} \hat{a}_{m'n} v^n_{j'k'}\right) \\ &\qquad = \sum_{n=1}^{N}\sum_{n'=1}^{N} v^n_{jk}\,\mathrm{cov}(\hat{a}_{mn}, \hat{a}_{m'n'})\, v^{n'}_{j'k'},\end{aligned} \tag{10}$$

and the variance of each time integral is

$$\sigma^2_{jkm} = \sum_{n=1}^{N}\sum_{n'=1}^{N} v^n_{jk}\,\mathrm{cov}(\hat{a}_{mn}, \hat{a}_{mn'})\, v^{n'}_{jk}. \tag{11}$$

Although the estimation of compartmental model kinetic parameters from the reconstructed time-activity curves is not considered here, kinetic parameters can be estimated more precisely using nonlinear weighted least squares, given the covariance between the time-activity curve models for the blood input function and the tissue volumes of interest [10, 11].

As a figure of merit related to the global precision of the time-activity curve model for volume of interest $m$, the following expression yields a squared noise-to-signal ratio (NSR) calculated as the mean (over all of the time segments) of the expected values of the squared errors between the integrated segments of the "true" and modeled curves, normalized by the mean square value of the integrated segments of the "true" curve:

$$\xi_m^2 = \frac{\sum_{j=1}^{J}\sum_{k=1}^{K}\sigma_{jkm}^2}{\sum_{j=1}^{J}\sum_{k=1}^{K}\left[\sum_{n=1}^{N}\hat{a}_{mn}v_{jk}^n\right]^2}. \tag{12}$$

Substituting equation (11) into equation (12), the squared NSR, $\xi_m^2$, can be calculated quickly by rearranging the summations, precomputing the inner products of the temporal basis functions, $\nu^{nn'} = \sum_{j=1}^{J}\sum_{k=1}^{K} v_{jk}^n v_{jk}^{n'}$, and exploiting the symmetry with respect to the indices $n$ and $n'$:

$$\xi_m^2 = \frac{\sum_{n=1}^{N}\sum_{n'=1}^{N}\operatorname{cov}(\hat{a}_{mn},\hat{a}_{mn'})\nu^{nn'}}{\sum_{n=1}^{N}\sum_{n'=1}^{N}\hat{a}_{mn}\hat{a}_{mn'}\nu^{nn'}}. \tag{13}$$

The global NSR, $\xi_m$, is used in Section III to assess the precision of temporal modeling for simulated dynamic cardiac cone beam SPECT studies.

## III. Computer Simulations

Using the simulation apparatus described in [4], Monte Carlo simulations were performed to validate the fast algorithm presented in Section II, and to study the effects of the temporal modeling on the statistical variability of the reconstructed spatiotemporal distributions

Simulated spatiotemporal distributions were obtained using the Mathematical Cardiac Torso (MCAT) phantom developed at the University of North Carolina [12]. The emission phantom (Fig. 1) was composed of 128 contiguous 1.75 mm-thick slices and contained the blood pool, three myocardial tissue volumes of interest (normal myocardium, septal defect, and lateral defect), liver, and background tissue. Projections were attenuated using the corresponding MCAT attenuation phantom.

The simulated time-activity curves (Fig. 2) mimicked the kinetics of teboroxime [13]. The simulated 15 min data acquisition consisted of $I = 2048$ cone beam projection rays per angle (64 transverse $\times$ 32 axial), $J = 120$ angles per revolution, and $K = 15$ revolutions, and thus yielded about 3.7 million projection samples. The projection bins were 7 mm $\times$ 7 mm at the detector, and the detector was 30 cm from the center of the field of view. The cone beam collimators had a hole diameter of 2 mm, a length of 4 cm, and were offset 1 cm from the detector. The focal length was 70 cm, which resulted in truncation of the data (Fig. 1). Attenuation and geometric point response were modeled using a ray-driven projector with line length weighting [14]. Scatter was not modeled. The amplitude of the simulated blood input function was adjusted so that about 10 million events were detected using the cone beam collimators.

The spatial basis projection factors $u_{ij}^m$ were defined by forward projecting each of the six known emission volumes composing the MCAT phantom (Fig. 1). Each emission volume was modeled to contain spatially uniform activity, which yielded $M = 6$ sets of spatial basis projection factors.

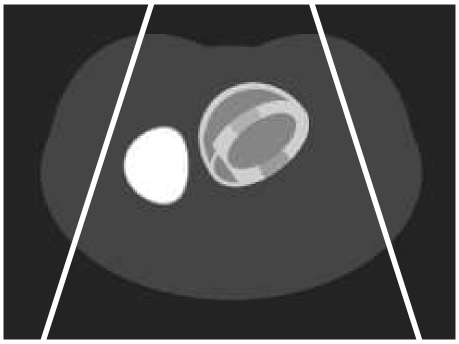

Fig. 1. Transverse cross section through the MCAT emission phantom, showing the truncation of data resulting from the use of cone beam collimators.

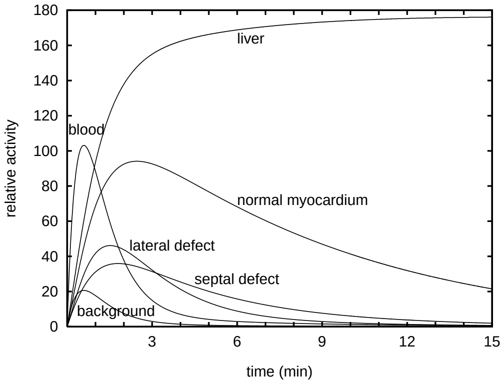


Fig. 2. Simulated teboroxime time-activity curves for the volumes in Fig. 1.

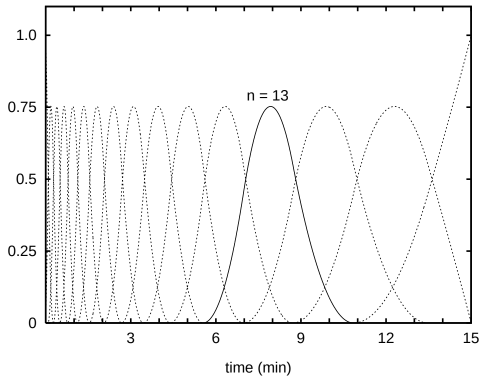


Fig. 3. Sixteen piecewise quadratic B-spline temporal basis functions used to validate the fast algorithm. The thirteenth spline is shown as a solid curve.

### A. Validation of the Fast Algorithm

A set of 1600 realizations of projection data having Poisson noise was generated and reconstructed using temporal basis integral factors $v_{jk}^n$ that were defined by integrating $N = 16$ splines spanning 15 time segments having geometrically increasing length (Fig. 3). Piecewise quadratic B-splines were used with an initial time segment length of 10 sec. The resulting curve models were continuous through their first derivative. For noiseless projections, the modeling error was less than 2%, where the error was defined to be the root mean square (RMS) difference between the simulated curve and the spline model,

TABLE I

OBSERVED AND ESTIMATED STATISTICAL UNCERTAINTIES FOR SPATIOTEMPORAL BASIS FUNCTION COEFFICIENTS, FOR 1600 REALIZATIONS OF NOISY PROJECTIONS. THE SAMPLE STANDARD DEVIATIONS OF THE COEFFICIENTS (THE SECOND COLUMN IN EACH OF THE FOUR SUB-TABLES) AGREE CLOSELY WITH THE SAMPLE MEANS OF THE ESTIMATED STATISTICAL UNCERTAINTIES (THE THIRD COLUMN IN EACH OF THE FOUR SUB-TABLES).

| $n$ | blood pool | | | normal myocardium | | | septal defect | | | lateral defect | | |
|---|---|---|---|---|---|---|---|---|---|---|---|---|
| | $\hat{a}_{1n}$ | | $\hat{\sigma}_{\hat{a}_{1n}}$ | $\hat{a}_{2n}$ | | $\hat{\sigma}_{\hat{a}_{2n}}$ | $\hat{a}_{3n}$ | | $\hat{\sigma}_{\hat{a}_{3n}}$ | $\hat{a}_{4n}$ | | $\hat{\sigma}_{\hat{a}_{4n}}$ |
| | sample mean | sample sdev | sample mean | sample mean | sample sdev | sample mean | sample mean | sample sdev | sample mean | sample mean | sample sdev | sample mean |
| 1 | 0.279 | 0.128 | 0.131 | 0.0102 | 0.166 | 0.166 | -0.0529 | 1.28 | 1.29 | -0.212 | 0.747 | 0.762 |
| 2 | 5.20 | 0.138 | 0.140 | 1.05 | 0.171 | 0.174 | 0.559 | 1.33 | 1.35 | 0.979 | 1.47 | 1.46 |
| 3 | 7.65 | 0.157 | 0.160 | 2.30 | 0.185 | 0.187 | 1.36 | 1.89 | 1.88 | 1.38 | 3.00 | 2.99 |
| 4 | 8.20 | 0.172 | 0.175 | 3.75 | 0.331 | 0.333 | 1.89 | 3.04 | 3.05 | 2.42 | 1.95 | 1.95 |
| 5 | 7.19 | 0.153 | 0.160 | 5.15 | 0.222 | 0.219 | 2.33 | 1.91 | 1.94 | 3.25 | 1.26 | 1.27 |
| 6 | 5.40 | 0.105 | 0.107 | 6.30 | 0.148 | 0.145 | 2.70 | 1.20 | 1.24 | 3.58 | 1.75 | 1.73 |
| 7 | 3.51 | 0.0974 | 0.0953 | 7.07 | 0.141 | 0.140 | 2.87 | 1.50 | 1.54 | 3.59 | 0.876 | 0.864 |
| 8 | 2.00 | 0.0658 | 0.0668 | 7.36 | 0.108 | 0.109 | 2.67 | 0.886 | 0.904 | 3.11 | 1.08 | 1.09 |
| 9 | 1.04 | 0.0545 | 0.0543 | 7.21 | 0.0839 | 0.0836 | 2.45 | 0.600 | 0.602 | 2.44 | 0.593 | 0.602 |
| 10 | 0.535 | 0.0464 | 0.0446 | 6.71 | 0.0743 | 0.0735 | 2.02 | 0.560 | 0.562 | 1.69 | 0.418 | 0.411 |
| 11 | 0.308 | 0.0361 | 0.0362 | 5.98 | 0.0632 | 0.0628 | 1.57 | 0.486 | 0.477 | 1.03 | 0.364 | 0.354 |
| 12 | 0.208 | 0.0305 | 0.0298 | 5.13 | 0.0538 | 0.0530 | 1.13 | 0.397 | 0.399 | 0.592 | 0.296 | 0.300 |
| 13 | 0.149 | 0.0250 | 0.0245 | 4.20 | 0.0454 | 0.0441 | 0.761 | 0.327 | 0.325 | 0.307 | 0.258 | 0.253 |
| 14 | 0.103 | 0.0197 | 0.0201 | 3.28 | 0.0360 | 0.0365 | 0.478 | 0.268 | 0.270 | 0.179 | 0.206 | 0.207 |
| 15 | 0.0657 | 0.0167 | 0.0168 | 2.39 | 0.0303 | 0.0308 | 0.268 | 0.232 | 0.234 | 0.0853 | 0.165 | 0.170 |
| 16 | 0.0399 | 0.0169 | 0.0169 | 1.64 | 0.0314 | 0.0313 | 0.135 | 0.270 | 0.269 | 0.0651 | 0.161 | 0.164 |

TABLE II

OBSERVED AND ESTIMATED NOISE-TO-SIGNAL RATIOS FOR TIME-ACTIVITY CURVES, FOR 1600 REALIZATIONS OF NOISY PROJECTIONS.

| | observed NSR (%) | | estimated NSR $\xi_m$ (%) | |
|---|---|---|---|---|
| | sample mean | sample sdev | sample mean | sample sdev |
| blood pool | 1.51 | 0.35 | 1.56 | 0.008 |
| normal myocardium | 1.13 | 0.27 | 1.16 | 0.003 |
| septal defect | 32.5 | 9.1 | 32.5 | 2.6 |
| lateral defect | 28.5 | 8.0 | 28.6 | 2.3 |
| liver | 0.167 | 0.031 | 0.170 | 0.0001 |
| background | 0.242 | 0.058 | 0.247 | 0.0002 |

normalized by the RMS value of the simulated curve [4].

The computational benefit of using the factorization given by equation (9) to estimate the covariance matrix for the spatiotemporal basis function coefficients was evident in the simulations. The number of multiply-and-add operations used to calculate $\mathbf{F}^{\mathrm{T}}\mathrm{diag}(\mathbf{F}\hat{\mathbf{a}})\mathbf{F}$ was reduced from about 17 billion to about 80 million. Using a 194-MHz R10000-based SGI workstation, it took 34 sec to estimate the 96 coefficients for the spatiotemporal basis functions, their covariance matrix, and the squared noise-to-signal ratios given by equation (13).

Table I shows that for the blood pool and myocardial tissue volumes, the sample means of the $\hat{\sigma}_{\hat{a}_{mn}}$ (the square roots of the diagonal elements of the estimated covariance matrix) were within 5% of the sample standard deviations of the $\hat{a}_{mn}$ (the estimated spatiotemporal basis function coefficients). For the liver and background tissue, the agreement was to within 4% (data not shown). The coefficients of variation for the $\hat{\sigma}_{\hat{a}_{mn}}$ were less than 2% (data not shown).

Table II shows that the sample means of the $\xi_m$ [the estimated NSRs given by equation (13)] were within 4% of the sample means of the RMS differences between the 1600 sets of time-activity curve models and their corresponding mean curves, normalized by the RMS values of the mean curves. The curves for the septal and lateral defects exhibited the largest variability, because of their small spatiotemporal support.

## *B. Effects of Temporal Modeling*

To study the statistical variability that results from modeling various orders of temporal continuity and using various time samplings, 24 sets of 1000 realizations of projection data having Poisson noise were generated. Each set of 1000 projections was reconstructed using a different set of temporal basis functions consisting of $N = 16$ splines spanning 15 time segments having geometrically increasing length (e.g., Fig. 3). Piecewise cubic, quadratic, linear, or constant B-splines were used with initial time segment lengths of 2.5, 5, 10, 20, 40, or 60 sec.

Fig. 4 shows the results for the blood pool and three myocardial tissue volumes. For each temporal basis set and volume of interest, there was close agreement between the sample mean of the estimated NSR, $\xi_m$, and the observed NSR, which was calculated as described in the caption for Fig. 4. The effect of the polynomial order of the splines on the NSR was relatively small, while the effect of the time sampling was larger. The NSR tended to decrease as the time sampling became more uniform (e.g., for initial time segment lengths of 40 or 60 sec). However, the decrease in NSR was offset by an increase in RMS bias, which was calculated as described in the caption for Fig. 4. The RMS bias increased because these basis sets had initial samplings that were too long to accurately model the beginning of the acquisition, when the activity concentrations were changing most rapidly (Fig. 2). The RMS bias also tended to increase as the polynomial order of the splines decreased. Overall, the best results were obtained with cubic or quadratic splines having initial time samplings of 10 sec or less. Similar findings were obtained for the liver and background tissue (data not shown).

## IV. DISCUSSION

The fast algorithm presented in Section II facilitated the study of the statistical variability that results from modeling various

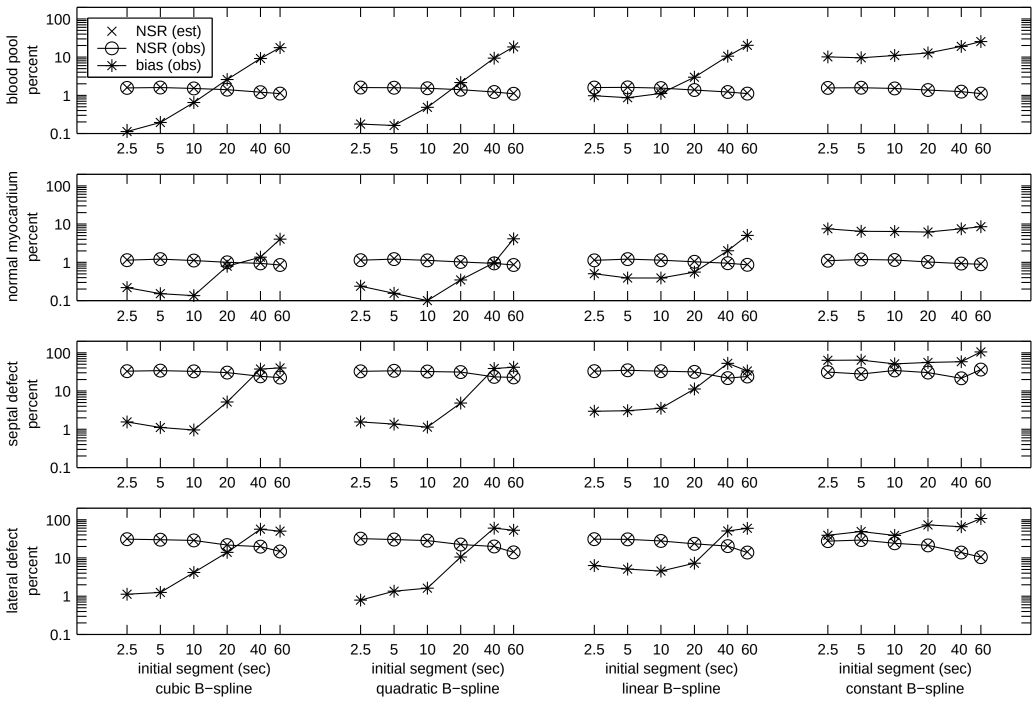


Fig. 4. Effects of temporal modeling. The "$*$" symbols denote RMS bias values observed for 1000 realizations of noisy projections. For each temporal basis set, RMS bias was calculated by first calculating the mean time-activity curve for the 1000 noisy curves, and then calculating the RMS difference between the mean noisy curve and the simulated curve (Fig. 2). The RMS difference was then normalized by the RMS value for the simulated curve and expressed as a percentage. The "$\circ$" symbols denote the observed NSR for each basis set, which was calculated as the mean value of the RMS differences between the 1000 noisy curves and the mean noisy curve, normalized by the RMS value of the mean noisy curve, and expressed as a percentage. The "$\times$" symbols denote the mean values of the estimated NSR, $\xi_m$, calculated using equation (13). These values agree closely with the observed NSR values.

orders of temporal continuity and using various time samplings, when estimating spatiotemporal distributions directly from dynamic SPECT projection data. The simulation results presented in Section III suggest that there is benefit in modeling higher orders of temporal continuity. In addition, it appears that the accuracy of time-activity curve models can be increased substantially without unduly increasing their statistical uncertainty, by using relatively fine initial time sampling to capture rapidly changing activity distributions.

Future work includes a study of the effects of the B-spline order and initial time sampling on nonlinear weighted least squares estimates of compartmental model kinetic parameters obtained from the time-activity curve models.

## ACKNOWLEDGMENT

The authors thank the University of North Carolina Medical Imaging Research Laboratory for making the MCAT phantom available. This work was supported by the National Heart, Lung, and Blood Institute of the US Department of Health and Human Services under grants R01-HL50663 and P01-HL25840 and by the Director, Office of Science, Office of Biological and Environmental Research, Medical Sciences Division of the US Department of Energy under contract DE-AC03-76SF00098. This work was developed in part using the resources at the US Department of Energy National Energy Research Scientific Computing (NERSC) Center.

## REFERENCES


[1] R. H. Huesman, B. W. Reutter, G. L. Zeng, and G. T. Gullberg, "Kinetic parameter estimation from SPECT cone-beam projection measurements," *Phys Med Biol*, vol. 43, no. 4, pp. 973–982, 1998.

[2] G. T. Gullberg, R. H. Huesman, S. G. Ross, E. V. R. Di Bella, G. L. Zeng, B. W. Reutter, P. E. Christian, and S. A. Foresti, "Dynamic cardiac single-photon emission computed tomography," in *Nuclear Cardiology: State of the Art and Future Directions*, B. L. Zaret and G. A. Beller, Eds., chapter 11, pp. 137–187. Mosby Inc., St. Louis, MO, 1999.

[3] A. Sitek, E. V. R. Di Bella, and G. T. Gullberg, "Reconstruction from slow rotation dynamic SPECT using a factor model," in *Information Processing in Medical Imaging: Proceedings of the Sixteenth International Conference*, A. Kuba, M. Šámal, and A. Todd-Pokropek, Eds., 1999, pp. 436–441.

[4] B. W. Reutter, G. T. Gullberg, and R. H. Huesman, "Direct least-squares estimation of spatiotemporal distributions from dynamic SPECT projections using a spatial segmentation and temporal B-splines," *IEEE Trans Med Imag*, vol. 19, no. 5, pp. 434–450, 2000.

[5] J. S. Maltz, "Direct recovery of regional tracer kinetics from temporally inconsistent dynamic ECT projections using dimension-reduced time-activity basis," *Phys Med Biol*, vol. 45, no. 11, pp. 3413–3429, 2000.

[6] A. Celler, T. Farncombe, C. Bever, D. Noll, J. Maeght, R. Harrop, and D. Lyster, "Performance of the dynamic single photon emission computed tomography (dSPECT) method for decreasing or increasing activity changes," *Phys Med Biol*, vol. 45, no. 12, pp. 3525–3543, 2000.

[7] T. Farncombe, A. Celler, C. Bever, D. Noll, J. Maeght, and R. Harrop, "The incorporation of organ uptake into dynamic spect (dSPECT) image reconstruction," *IEEE Trans Nucl Sci*, vol. 48, no. 1, pp. 3–9, 2001.

[8] D. J. Kadrmas and G. T. Gullberg, "4D maximum *a posteriori* reconstruction in dynamic SPECT using a compartmental model-based prior," *Phys Med Biol*, vol. 46, no. 5, pp. 1553–1574, 2001.

[9] A. R. Formiconi, "Least squares algorithm for region-of-interest evaluation in emission tomography," *IEEE Trans Med Imag*, vol. 12, no. 1, pp. 90–100, 1993.

[10] R. H. Huesman and B. M. Mazoyer, "Kinetic data analysis with a noisy input function," *Phys Med Biol*, vol. 32, no. 12, pp. 1569–1579, 1987.

[11] D. J. Kadrmas, E. V. R. Di Bella, R. H. Huesman, and G. T. Gullberg, "Analytical propagation of errors in dynamic SPECT: Estimators, degrading factors, bias and noise," *Phys Med Biol*, vol. 44, no. 8, pp. 1997–2014, 1999.

[12] B. M. W. Tsui, J. A. Terry, and G. T. Gullberg, "Evaluation of cardiac cone-beam single photon emission computed tomography using observer performance experiments and receiver operating characteristic analysis," *Invest Radiol*, vol. 28, no. 12, pp. 1101–1112, 1993.

[13] R. K. Narra, T. Feld, and A. D. Nunn, "Absorbed radiation dose to humans from technetium-99m-teboroxime," *J Nucl Med*, vol. 33, no. 1, pp. 88–93, 1992.

[14] G. L. Zeng, G. T. Gullberg, B. M. W. Tsui, and J. A. Terry, "Three-dimensional iterative reconstruction algorithms with attenuation and geometric point response correction," *IEEE Trans Nucl Sci*, vol. 38, no. 2, pp. 693–702, 1991.